

Terrestrial ecosystem model performance in simulating productivity and its vulnerability to climate change in the northern permafrost region

J. Xia, A.D. Mcguire, D. Lawrence, E. Burke, G. Chen, X. Chen, C. Delire, C. Koven, A. Macdougall, S. Peng, et al.

▶ **To cite this version:**

J. Xia, A.D. Mcguire, D. Lawrence, E. Burke, G. Chen, et al.. Terrestrial ecosystem model performance in simulating productivity and its vulnerability to climate change in the northern permafrost region. Journal of Geophysical Research, 2017, 122 (2), pp.430-446. 10.1002/2016JG003384 . hal-01872578

HAL Id: hal-01872578
https://hal.science/hal-01872578

Submitted on 12 Sep 2018

HAL is a multi-disciplinary open access archive for the deposit and dissemination of scientific research documents, whether they are published or not. The documents may come from teaching and research institutions in France or abroad, or from public or private research centers.

L'archive ouverte pluridisciplinaire **HAL**, est destinée au dépôt et à la diffusion de documents scientifiques de niveau recherche, publiés ou non, émanant des établissements d'enseignement et de recherche français ou étrangers, des laboratoires publics ou privés.

AGU PUBLICATIONS

JGR

Journal of Geophysical Research: Biogeosciences

RESEARCH ARTICLE

10.1002/2016JG003384

Key Points:
- Current land models generate very high NPP over the permafrost regions, which mainly results from the overestimated CUE in the models
- Modeled GPP is comparable to flux tower-based estimate, but there is a twofold discrepancy among models
- Models highly varied in their sensitivities of NPP, GPP, and CUE to historical changes in climate and atmospheric CO_2 concentration

Supporting Information:
- Supporting Information S1
- Table S1

Correspondence to:
J. Xia and Y. Luo,
jyxia@des.ecnu.edu.cn;
yluo@ou.edu

Citation:
Xia, J., et al. (2017), Terrestrial ecosystem model performance in simulating productivity and its vulnerability to climate change in the northern permafrost region, *J. Geophys. Res. Biogeosci.*, *122*, 430–446, doi:10.1002/2016JG003384.

Received 17 FEB 2016
Accepted 24 JAN 2017
Accepted article online 26 JAN 2017
Published online 22 FEB 2017

©2017. American Geophysical Union. All Rights Reserved.

Terrestrial ecosystem model performance in simulating productivity and its vulnerability to climate change in the northern permafrost region

Jianyang Xia[1], A. David McGuire[2], David Lawrence[3], Eleanor Burke[4], Guangsheng Chen[5], Xiaodong Chen[6], Christine Delire[7], Charles Koven[8], Andrew MacDougall[9], Shushi Peng[10,11,12], Annette Rinke[13,14], Kazuyuki Saito[15], Wenxin Zhang[16], Ramdane Alkama[7], Theodore J. Bohn[6], Philippe Ciais[10], Bertrand Decharme[7], Isabelle Gouttevin[11,12,17], Tomohiro Hajima[15], Daniel J. Hayes[18], Kun Huang[1], Duoying Ji[13], Gerhard Krinner[11,12], Dennis P. Lettenmaier[6], Paul A. Miller[19], John C. Moore[13], Benjamin Smith[19], Tetsuo Sueyoshi[20,21], Zheng Shi[22], Liming Yan[1], Junyi Liang[22], Lifen Jiang[22], Qian Zhang[13], and Yiqi Luo[22,23]

[1]Research Center for Global Change and Ecological Forecasting and Tiantong National Field Observation Station for Forest Ecosystem, School of Ecological and Environmental Sciences, East China Normal University, Shanghai, China, [2]U.S. Geological Survey, Alaska Cooperative Fish and Wildlife Research Unit, University of Alaska Fairbanks, Fairbanks, Alaska, USA, [3]National Center for Atmospheric Research, Boulder, Colorado, USA, [4]Met Office Hadley Centre, Exeter, UK, [5]Environmental Sciences Division, Oak Ridge National Laboratory, Oak Ridge, Tennessee, USA, [6]Department of Civil and Environmental Engineering, University of Washington, Seattle, Washington, USA, [7]CNRM, Unitémixte de recherche CNRS/Meteo-France (UMR 3589), Toulouse, France, [8]Lawrence Berkeley National Laboratory, Berkeley, California, USA, [9]School of Earth and Ocean Sciences, University of Victoria, Victoria, British Columbia, Canada, [10]Laboratoire des Sciences du Climat et de l'Environnement, CEA-CNRS-UVSQ, UMR8212, Gif-sur-Yvette, France, [11]CNRS, Laboratoire de Glaciologie et Géophysique de l'Environnement (LGGE), Grenoble, France, [12]Université Grenoble Alpes and LGGE, Grenoble, France, [13]College of Global Change and Earth System Science, Beijing Normal University, Beijing, China, [14]Alfred Wegener Institute Helmholtz Centre for Polar and Marine Research, Potsdam, Germany, [15]Department of Integrated Climate Change Projection Research, Japan Agency for Marine-Earth, Yokohama, Japan, [16]Center for Permafrost (CENPERM), Department of Geosciences and Natural Resource Management, University of Copenhagen, Copenhagen, Denmark, [17]Irstea, UR HHLY, Villeurbanne, France, [18]School of Forest Resources, University of Maine, Orono, Maine, USA, [19]Department of Physical Geography and Ecosystem Science, Lund University, Lund, Sweden, [20]National Institute of Polar Research, Tachikawa, Japan, [21]Project Team for Risk Information on Climate Change, Japan Agency for Marine-Earth Science and Technology, Yokohama, Japan, [22]Department of Microbiology and Plant Biology, University of Oklahoma, Norman, Oklahoma, USA, [23]Department for Earth System Science, Tsinghua University, Beijing, China

Abstract Realistic projection of future climate-carbon (C) cycle feedbacks requires better understanding and an improved representation of the C cycle in permafrost regions in the current generation of Earth system models. Here we evaluated 10 terrestrial ecosystem models for their estimates of net primary productivity (NPP) and responses to historical climate change in permafrost regions in the Northern Hemisphere. In comparison with the satellite estimate from the Moderate Resolution Imaging Spectroradiometer (MODIS; 246 ± 6 g C m^{-2} yr^{-1}), most models produced higher NPP (309 ± 12 g C m^{-2} yr^{-1}) over the permafrost region during 2000–2009. By comparing the simulated gross primary productivity (GPP) with a flux tower-based database, we found that although mean GPP among the models was only overestimated by 10% over 1982–2009, there was a twofold discrepancy among models (380 to 800 g C m^{-2} yr^{-1}), which mainly resulted from differences in simulated maximum monthly GPP (GPP_{max}). Most models overestimated C use efficiency (CUE) as compared to observations at both regional and site levels. Further analysis shows that model variability of GPP and CUE are nonlinearly correlated to variability in specific leaf area and the maximum rate of carboxylation by the enzyme Rubisco at 25°C (V_{cmax_25}), respectively. The models also varied in their sensitivities of NPP, GPP, and CUE to historical changes in climate and atmospheric CO_2 concentration. These results indicate that model predictive ability of the C cycle in permafrost regions can be improved by better representation of the processes controlling CUE and GPP_{max} as well as their sensitivity to climate change.

1. Introduction

Permafrost regions in the Northern Hemisphere store a huge amount of carbon (C) and play a critical role in regulating terrestrial feedbacks to climate change [*Schuur et al.*, 2008; *McGuire et al.*, 2009; *Tchebakova et al.*, 2009;

Schaefer et al., 2014; *Schuur et al*., 2015]. However, the key C processes in permafrost regions have not been well represented and evaluated in terrestrial ecosystem models, partially leading to the large uncertainty in future projections of climate-C cycle feedbacks by Earth system models [*Koven et al*., 2011; *Friedlingstein et al*., 2013; *Schaefer et al*., 2014; *Koven et al*., 2015]. Net primary productivity (NPP), the total net C influx into an ecosystem, is the key C process determining C stock in permafrost regions [*McGuire et al*., 2010]. Previous model intercomparison exercises have emphasized the importance of NPP in simulations of the stimulate global carbon cycle [*Todd-Brown et al*., 2013; *Hajima et al*., 2014], but a spread of twofold to threefold in simulated global NPP has been revealed since the late 1990s [*Cramer et al*., 1999], e.g., 35.3 to 91.3 Pg C yr^{-1} among CMIP5 models [*Todd-Brown et al*., 2013]. In comparison with the global average, the CMIP5 models have much larger disparity in simulated NPP for boreal forest (fourfold; 2.3–9.1 Pg C yr^{-1}) and tundra (sixteenfold; 0.3–4.7 Pg C yr^{-1}) [*Todd-Brown et al*., 2013], biomes which are mainly located in the northern permafrost region. Thus, identification of systematic biases in carbon cycle models for simulating NPP in permafrost regions can be instructive to enhance the skill of Earth ecosystem models.

NPP can be decomposed as the product of gross primary productivity (GPP) and carbon use efficiency (CUE; the ratio of NPP to GPP). Most previous efforts focused on diagnosing differences in simulated NPP among models have primarily analyzed differences in GPP. There is a large difference among the CMIP5 models' simulation of contemporary global total terrestrial GPP, which ranges from 105.3 to 176.9 Pg C [*Anav et al*., 2013]. In the latest two Intergovernmental Panel on Climate Change Assessment Reports, substantial uncertainties have been revealed by carbon cycle models with the same climate forcing in simulated GPP responses to changes in climate and atmospheric CO_2, with 0.8–7.6 Pg C yr^{-1} per 100 mm precipitation, −2.5 to 2.0 Pg C yr^{-1} $°C^{-1}$, and 8.1–30.0 Pg C yr^{-1} per 100 ppmv to increases in global total annual precipitation, mean annual temperature, and atmospheric CO_2 concentration, respectively [*Piao et al*., 2013]. The CUE, which describes the capacity of an ecosystem to transfer assimilated C to biomass [*Cheng et al*., 2000; *DeLucia et al*., 2007; *Bradford and Crowther*, 2013; *Dillaway and Kruger*, 2014], is a conceptually simple ratio, but it varies with climate [*Metcalfe et al*., 2010; *Dillaway and Kruger*, 2014; *Zhang et al*., 2014], stand age [*Piao et al*., 2010], and vegetation type [*Litton et al*., 2007; *Zhang et al*., 2009]. Also, the models have diverse representations of the allocation of NPP to different plant tissues [*De Kauwe et al*., 2014], which in turn could affect CUE because of the different respiratory demands among those plant tissues. Hence, it is important to evaluate (1) whether the factors affecting CUE have been well represented by the models and (2) the relative contributions of GPP and CUE to the large uncertainty in NPP estimates among models.

In this study, we examine 10 process-based models for their ability to estimate NPP and its response to climate change in permafrost regions of the Northern Hemisphere from a series of retrospective simulations during 2000–2009. We aim to address the following questions: (1) Does CUE contribute to the differences in NPP among models and between data products and model outputs? If so, how? (2) What are the key sources of the intermodel variations of simulated GPP and CUE in the permafrost region? and (3) What is the relative importance of air temperature, precipitation, and atmospheric CO_2 in regulating the temporal trend of simulated NPP since 1960 across the permafrost region?

2. Materials and Methods

2.1. Model Input Data and Simulation Experiments

The primary focus of this study is to evaluate NPP, GPP, and CUE simulated by 10 terrestrial ecosystem models (Table 1) that have participated in the activities of the model integration group of the Permafrost Carbon Network (http://www.permafrostcarbon.org/). The model ensemble includes CLM4.5 [*Koven et al*., 2013; *Oleson et al*., 2013], CoLM [*Dai et al*., 2003; *Ji et al*., 2014], ISBA [*Gibelin et al*., 2006], JULES [*Clark et al*., 2011], LPJ-GUESS [*Smith et al*., 2001], MIROC-ESM [*Sato et al*., 2007; *Watanabe et al*., 2011], ORCHIDEE [*Krinner et al*., 2005], TEM6 [*Zhuang et al*., 2003; *Hayes et al*., 2011], UVic [*Cox*, 2001; *Matthews et al*., 2004], and UW-VIC [*Knorr*, 2000; *Bohn et al*., 2007]. A description of the 10 models can be found in *Rawlins et al*. [2015] and *McGuire et al*. [2016]. The calculations of growth and maintenance respiration as well as photosynthetic capacity (V_{cmax}) for different models are shown in Table S1 in the supporting information. A detailed description of the prescribed plant functional type (PFT) (Figure S1) and associated parameterizations of specific leaf area (SLA) and the maximum rate of carboxylation by the enzyme Rubisco at 25°C (V_{cmax_25}) in each model is provided in Table S2. Different approaches have been applied to model soil thermal

Table 1. A Brief Comparison of Conceptual Representation of Processes Affecting NPP Among the 10 Models

Model	Dynamic Vegetation	Light Limitation	N Limitation	CO_2 Effect	Prognostic Ra[a]	Prognostic LAI[a]
CLM45	Yes	Yes	Yes	No	Yes	Yes
CoLM	Yes	Yes	No	No	Yes	Yes
ISBA	No	Yes	No	Yes	Yes	Yes
JULES	No	Yes	No	Yes	Yes	Yes
LPJ-GUESS	Yes	Yes	Yes	Yes	Yes	Yes
MIROC-ESM	Yes	Yes	No	No	Yes	Yes
ORCHIDEE	Yes	Yes	No	No	Yes	Yes
TEM6	No	Yes	No	No	Yes	Yes
UVic	Yes	Yes	No	No	Yes	Yes
UW-VIC	No	Yes	Yes	No	Yes	No

[a]Ra, autotrophic respiraiton; LAI, leaf area index.

dynamics [*Peng et al*., 2016], and the information on these approaches are provided by *McGuire et al*. [2016]. The models were run retrospectively from 1960 to 2009 at 0.5° × 0.5° spatial resolution over the northern permafrost region (Figure 1). The spatial domain of permafrost region includes five subregions: boreal Asia (BOAS), boreal Europe (BOEU), boreal North America (BONA), other permafrost areas (Other), and glaciers/ice sheets. Each model was allowed to choose appropriate driving data sets for atmospheric CO_2, N deposition, climate, disturbance, and other forcings. The different forcing data sets for climate and other model boundary conditions collectively represent both uncertainty from climate forcing (and other forcings) and from model parameterization and structure in simulating C dynamics across the permafrost region. As analyzed by *McGuire et al*. [2017], there were little differences in the atmospheric CO_2 concentrations used to drive the models, and the trend in annual air temperature across the permafrost regions from 1960 to

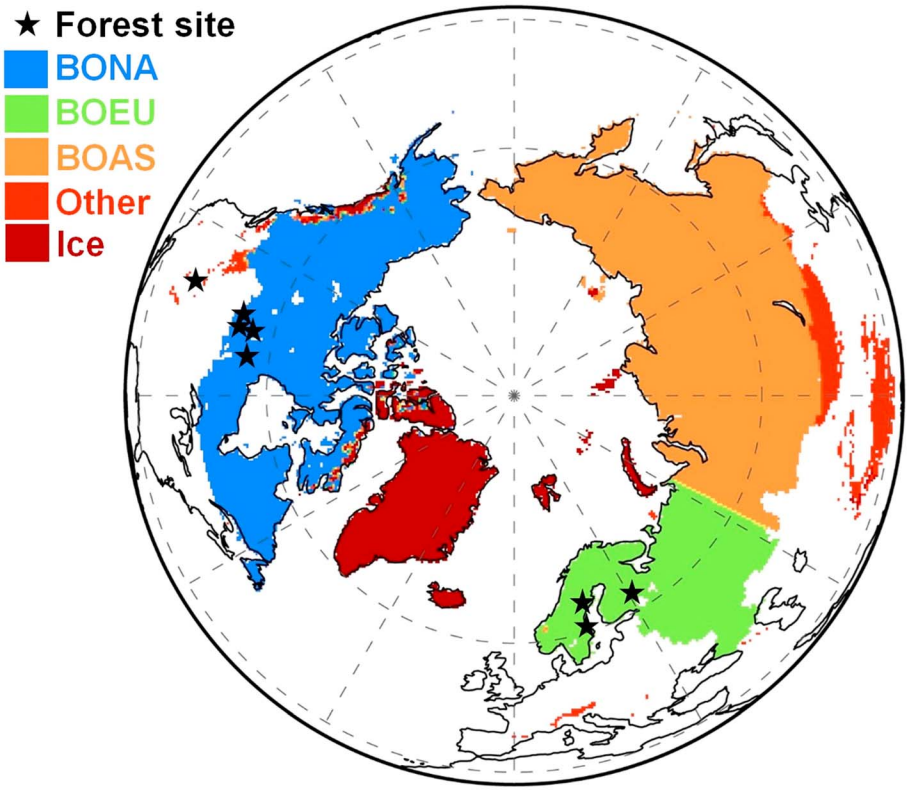


Figure 1. The spatial domain of permafrost region in the Northern Hemisphere defined in this study. The permafrost region includes five subregions, including boreal Asia (BOAS), boreal Europe (BOEU), boreal North America (BONA), other permafrost areas (Other), and Glaciers and Ice Sheets (Ice). The black stars represent the forest sites in the northern permafrost region with both GPP and NPP data from a global database [*Luyssaert et al*., 2007].

2009 was the same for all models (0.03°C yr^{-1}). Precipitation trends from 1960 to 2009 across the permafrost regions varied substantially among the model (−2.1 to 0.8 mm yr^{-1}). Although long-wave radiation trend is important for changes in soil temperature in the models [*Peng et al.*, 2015], it is not related to change in permafrost area.

To better understand the sensitivity of the models to historical changes in climate, including atmospheric CO_2, temperature, and precipitation, four simulation experiments were conducted to determine the relative contributions of these drivers on C cycle changes during 1960–2009. These experiments were (1) all historical forcing data (all input data kept changing through time; the baseline simulation R01), (2) constant temperature (detrended temperature from 1960 to 2009 with all other input data kept changing with time; the R02 simulation), (3) constant CO_2 (the R03 simulation), and (4) constant temperature and precipitation (the R04 simulation). The effect of temperature, CO_2, and precipitation on C processes was estimated via R02 − R01, R03 − R01, and R04 − R02, respectively.

2.2. Satellite-Derived NPP Data

Satellite-derived NPP data from the MODIS aboard the National Aeronautics and Space Administration Terra satellite (MOD17A3 NPP) were used to evaluate the modeled NPP [*Heinsch et al.*, 2003]. The data product (available from the Land Processes Distributed Active Archive Center; https://lpdaac.usgs.gov/dataset_discovery/modis/modis_products_table/mod17a3) was generated by Numerical Terradynamic Simulation Group/University of Montana as Version-55 [*Running and Zhao*, 2015] and included global NPP estimates since 2000 at 1 × 1 km resolution and on an annual basis. The accuracy of this data product, which corrects for cloud contamination, has been assessed and widely used to evaluate biogeochemical processes in northern permafrost regions [e.g., *Tuanmu and Jetz*, 2015; *Mao et al.*, 2015]. Since the MODIS NPP is estimated based on a light-use efficiency algorithm driven by fixed parameters within each biome type, it inevitably will lead to uncertainty in temporal and spatial variations. The daily meteorological inputs to MOD17 algorithm is derived from the global meteorological reanalysis data provided by Global Modeling and Assimilation Office/NASA [*Running and Zhao*, 2015]. The mean ratio of root-mean-square error (RMSE) of MOD17 NPP to mean measured NPP is 0.26, ranging from 0.13 to 0.53, across different vegetation types [*Turner et al.*, 2006]. In this study, the MOD17A3 NPP estimates were compared to the multiple-year average of NPP over 2000–2009 as simulated by the models. The data were mosaicked and reprojected by using the MODIS Reprojection Tool and mosaicked images resampled into 0.5° × 0.5° (latitude × longitude) resolution by using the nearest neighbor algorithm.

2.3. Data-Oriented GPP Estimates

To maintain independence between NPP and GPP data, a global monthly gridded GPP data product derived from FLUXNET measurements with a machine learning technique termed model tree ensemble (MTE) [*Jung et al.*, 2011] was used to evaluated the modeled GPP over 1982–2009. The MTE approach statistically scales up the FLUXNET GPP (about 20 sites are located in the permafrost region as shown by Figure 1) to a spatial resolution of 0.5° × 0.5° by integrating satellite-derived indices, meteorological data, and land use information [*Jung et al.*, 2011] (hereafter JU11 GPP). The global grids of monthly precipitation in JU11 algorithm were from Global Precipitation Climatology Centre [*Schneider et al.*, 2008] The JU11 GPP data product has a relatively small uncertainty (about 119 ± 6 Pg C yr^{-1}globally) and has been widely used for benchmarking model performance in recent years [*Anav et al.*, 2013; *Piao et al.*, 2013; *Tjiputra et al.*, 2013; *Peng et al.*, 2015].

2.4. Carbon Use Efficiency

The CUE was calculated as NPP divided by GPP at both regional and site scales. The regional distribution of CUE was calculated from the MODIS NPP and JU11 GPP at the 0.5° × 0.5° resolution. Based on a global database of forest GPP and NPP [*Luyssaert et al.*, 2007], we selected eight sites which are located in the study region and had measurements for both GPP and NPP (Figure 1). Annual mean GPP and NPP were used for the calculation if there are multiple years of measurements. The database was established based on published literatures, existing data sets [*Olson et al.*, 2001; *Papale et al.*, 2006], and measurements from FLUXNET [*Baldocchi et al.*, 2001]. In this study, NPP and GPP in the eight forest sites were measured in natural conditions without any manipulative treatments [*Tang et al.*, 2014]. NPP in the database include aboveground and belowground NPP and was obtained directly from harvest or indirectly from biometric methods at most sites. NPP was estimated with process-based models with calibration and/or validation against

biomass observations at about 5% of the total sites. A more detailed description of the NPP methodologies can be found in *Campioli et al.* [2015]. GPP was mostly estimated from eddy covariance (73% of the sites) or process-based models with data calibration or validation (20% of the sites).

2.5. Analytical Methods

Due to the diverse resolution of original outputs from the models, we aggregated monthly outputs of NPP and GPP data from all models to 0.5° × 0.5° spatial resolution. We used a relative importance analysis approach to quantify the relative contributions of temperature, CO_2, and precipitation changes to dynamics of GPP and CUE over 1960–2009. This analysis was conducted using the "relaimpo" package in *R*, which is based on variance decomposition for multiple linear regression models [*Gromping*, 2006]. The relaimpo package provides six different methods for analyzing relative importance of each regressor in linear regression. We chose one of the most computer-intensive and commonly used methods named "lmg," which averages the sequential sum of squares for all possible orders of terms to estimate the percentage of the variance from each term [*Linderman et al.*, 1980]. The relaimpo package has been widely used for separating the relative roles of various factors in ecological studies in recent years [*Sonnentag et al.*, 2010; *Wu et al.*, 2013; *Belmaker and Jetz*, 2015; *Fernandez-Martinez et al.*, 2015]. Since MODIS NPP and JU11 GPP were derived from satellite- and flux-based data, respectively, each has uncertainties. Given that the percentage of true observations within one or two standard deviation of JU11 estimates was 73% and 90%, respectively [*Jung et al.*, 2009], we assumed a 20% uncertainty for both data sets at 0.5° resolution and then applied a random sampling (with sample size of 500) to estimate the CUE.

3. Results

3.1. Biases of NPP as Determined by GPP and CUE

The estimated mean annual NPP of the northern permafrost region during 1960–2009 by the 10 models was 285 ± 69 g C m^{-2} yr^{-1} (±SD of NPP among models), ranging from 198 ± 12 g C m^{-2} yr^{-1} (±SD of NPP over years) in LPJ-GUESS to 434 ± 27 g C m^{-2} yr^{-1} in ORCHIDEE (Figure 2a). Most models produced higher values than the MODIS NPP over 2000–2009, leading to an ensemble model average NPP that is about 20% higher than the MODIS NPP over 2000–2009 (Figure 2b).

The differences among models and biases from observed NPP can be decomposed into biases of GPP and CUE. As shown in Figure 2c, although there was also an approximately twofold difference (380 ± 24 g C m^{-2} yr^{-1} in LPJ-GUESS to 800 ± 49 g C m^{-2} yr^{-1} in ORCHIDEE) in averaged annual GPP among the models, the multimodel ensemble mean GPP was only 10% higher than the JU11 average GPP over 1982–2009 (Figure 2d). It suggests that the high values of NPP from most models reflect large values of CUE. As shown in Figure 3a, with an assumed uncertainty of 20% for both MODIS NPP and JU11 GPP, the estimated CUE ranged from 29% to 58% over 2000–2009. Two models, i.e., UW-VIC (68%) and ISBA (63%), had larger CUE than that estimated from MODIS NPP and JU11 GPP. The estimated CUE had very small variation in all process-based models. As compared to the observations (45 ± 4%; ±SE of CUE across sites) from eight forest sites in a global data set [*Luyssaert et al.*, 2007], most models overestimated CUE in the grid pixels including those sites (Figure 3b).

The CUE is determined by GPP and respiration, both of which are directly or indirectly affected by leaf area and leaf level photosynthetic capacity (e.g., V_{cmax}) (Table S1). The key parameters, such as SLA and V_{cmax_25}, are not the same among the models (Table S2), and they contribute to the NPP variation among models in different ways. As shown in Figure 4, SLA was nonlinearly correlated with GPP_{max} ($R^2 = 0.90$, $P = 0.01$), while V_{cmax_25} contributed to NPP variation among models by affecting CUE ($R^2 = 0.70$, $P = 0.09$).

3.2. Temporal and Spatial Variability of GPP Model Performance

The low interannual variability of CUE derived from the simulations indicated that the temporal variation of simulated NPP is mainly determined by variations of GPP in the models. As shown in Figure 5, the 10 models agreed well that GPP was initiated in March and terminated in November. Although the ensemble model mean monthly GPP was similar to the seasonal pattern of the JU11 data, there was an approximately twofold difference in the maximum monthly GPP among models, varying from 91 ± 5 g C m^{-2} month^{-1} in LPJ-GUESS to 205 ± 12 g C m^{-2} month^{-1} in ORCHIDEE (Figure 5a). Linear regression analysis showed that the model-to-model difference in annual GPP was well explained by the seasonal maximum GPP (GPP_{max}; $R^2 = 0.78$,

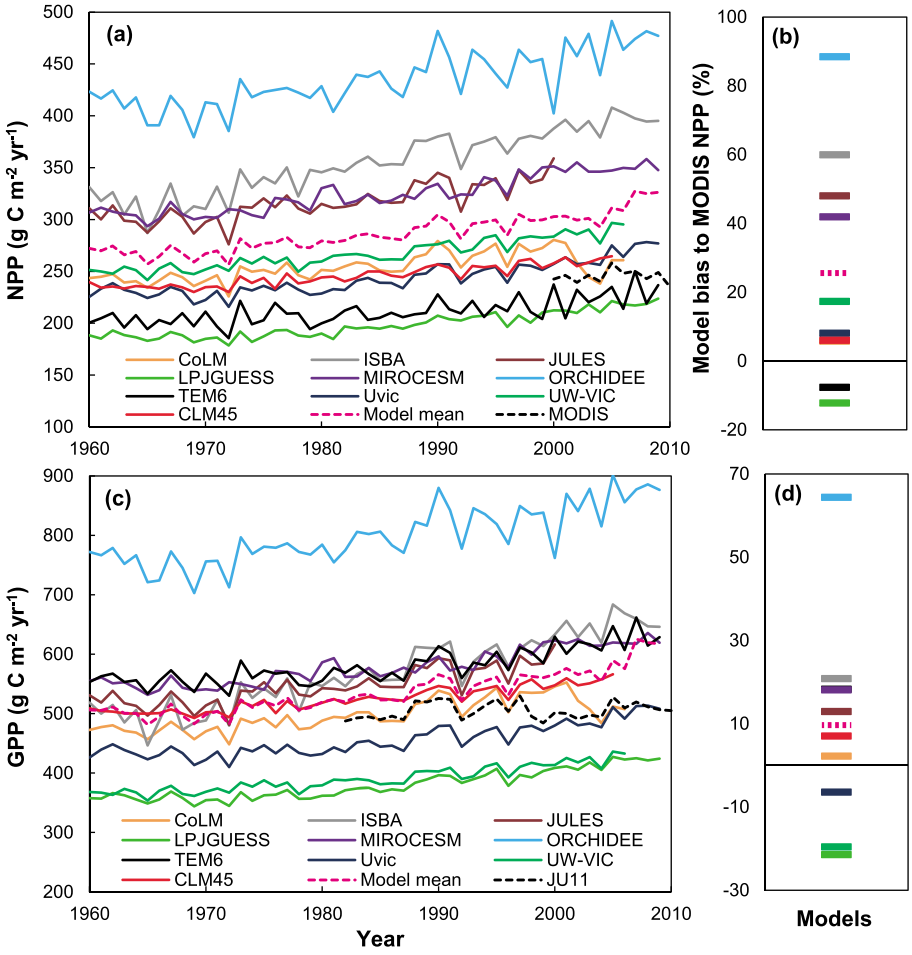


Figure 2. Yearly averaged (a) NPP and (c) GPP over permafrost region in the Northern Hemisphere since 1960 from models and data sets. Note that the MODIS NPP data are plotted since 2000 and the JU11 GPP data are plotted since 1982. The model biases of (b) NPP (over 2000–2009) and (d) GPP (over 1982–2009) are represented by the relative differences between model results and MODIS NPP and JU11 GPP estimates, respectively.

$P < 0.001$; Figure 5b). We further found that the variation in GPP_{max} was associated with variation in SLA rather than V_{cmax_25} among the models (Figure 4).

Spatially, the modeled annual GPP decreased along with increasing latitudes (Figure 6). Simulated GPP was higher than $450\,g\,C\,m^{-2}\,yr^{-1}$ over about 90% of the BOEU subregion, whereas it was less than $450\,g\,C\,m^{-2}\,yr^{-1}$ over 55%, 51%, and 74% of the BONA, BOAS, and Other subregions, respectively (Figure S2c). The model-to-model difference in annual GPP was especially greater in the lower latitude regions (Figure 6). The spatial pattern of model ensemble mean GPP was similar to that of the JU11 data (Figure S2a), except for the regions at latitudes lower than 35°N (Figure 6). These regions were mainly located in the Tibet Plateau, where the coefficient of variance (CV; CV = 100% × SD/mean) of GPP among models was high (21% of area-weighted CV among models over the permafrost region) (Figure S2d) but the GPP value was low (7% of area-weighted GPP over the permafrost region) (Figure S3c). However, the distributions of the ensemble model biases are similar across the study regions (Figure S3d).

3.3. Relative Contributions of Temperature, CO_2 and Precipitation to NPP Changes

All the 10 models show an increasing trend of annual NPP from 1960 to 2009 (Figure 2). Based on the six models that provided outputs for simulation experiments R02–04, we found that the increase in ensemble mean NPP over 1960–2009 predominantly resulted from increasing air temperature and atmospheric CO_2 concentration, while precipitation change showed nearly neutral contribution (Figures 7a–7c). Note that radiation trend may also have significant contribution to NPP changes [*Peng et al.*, 2015], but this study only focuses

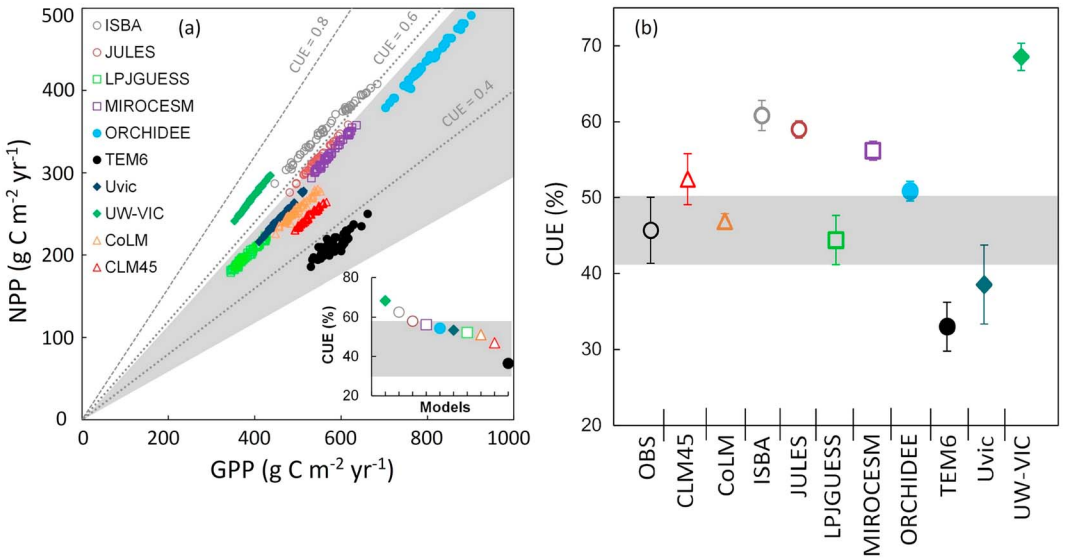


Figure 3. Carbon use efficiency (CUE), as calculated by dividing NPP by GPP. (a) Each data point represents one year since 1960. The shaded gray area is the calculated standard deviation (SD) of CUE based on MODIS NPP and JU11 GPP. In the insert panel, each symbol represents the temporal average of CUE for one model, and the dashed line is the calculated mean CUE based on MODIS NPP and JU11 GPP for 2000–2009. Note that the model symbols are shared by the main and insert panels. (b) Comparison of model-derived CUE (mean ± SE) with observation-derived CUE from the eight forest sites in the northern permafrost region from the database of *Luyssaert et al.* [2007]. The dashed line represents the mean CUE derived from the observations.

on the contributions of temperature, CO_2, and precipitation changes [*McGuire et al.*, 2016]. Although all the six models showed negative effects of temperature on CUE (Figure 7g), its changing magnitudes were not large enough to negate the positive effects of temperature change on GPP (Figure 7d). The positive impact of temperature change on GPP is produced by almost all the models except for the UVic model (Figure 7d). Increasing CO_2 enhanced both GPP (Figure 7e) and CUE (Figure 7h), leading to a positive effect on NPP over 1960–2009 (Figure 7b). For precipitation change, there was no clear trend for either GPP (Figure 7f) or CUE (Figure 7i).

We applied the relative importance analysis to separate the effects of temperature, CO_2, and precipitation changes on GPP and CUE over 1960–2009 (Figure 8). The results show that four (LPJ-GUESS, ORCHIDEE, TEM6, and UW-VIC) out of the six models produced very similar contributions of temperature, CO_2, and

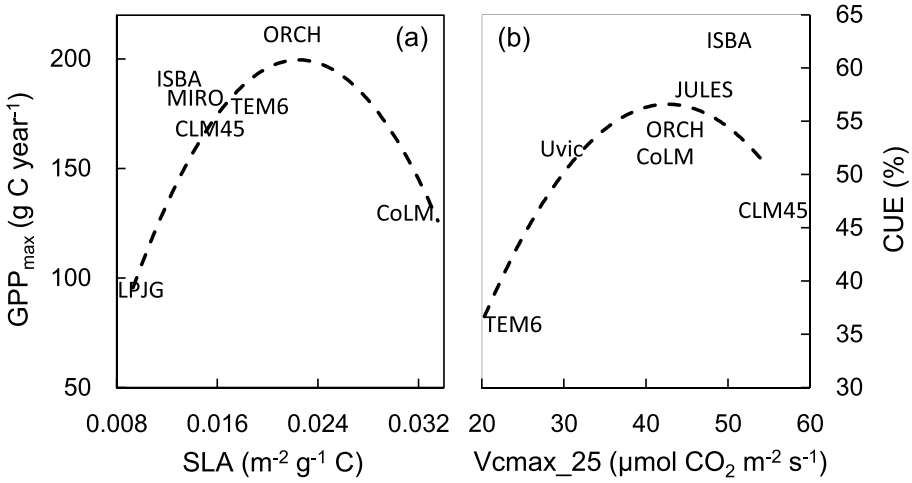


Figure 4. Dependences of (a) GPP_{max} on SLA and (b) CUE on V_{cmax_25} among models. Note that the medians of SLA and V_{cmax_25} across the permafrost region in each model were used in the regression analyses ($GPP_{max} = -568678SLA^2 + 25760SLA - 92$; $CUE = -0.04V_{cmax_25}^2 + 3.39V_{cmax_25} - 15.80$).

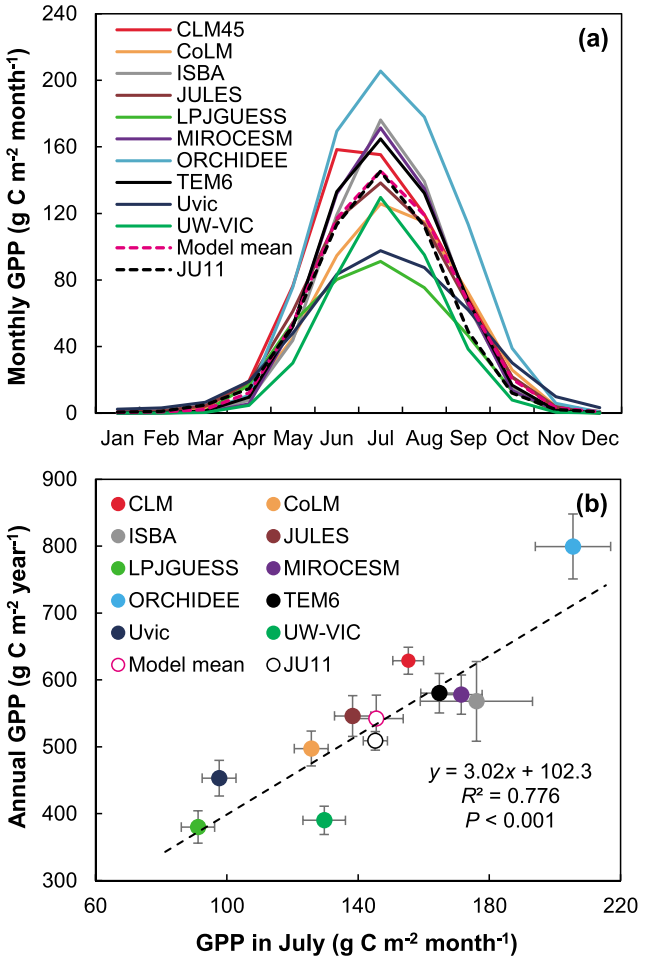


Figure 5. (a) Monthly dynamics of GPP for the northern permafrost region from model and JU11 estimates. (b) The relationship between annual total GPP and GPP in July among the models.

precipitation changes on GPP. The increasing GPP in the JULES model mainly resulted from CO_2 effect (~81%), whereas only the UVic model estimated a greater contribution from precipitation (~39%) to its GPP increase over 1960–2009 (Figure 8a). For the CUE changes, there were large model-to-model differences in the relative contributions of CO_2 (from 8% in UVic to 53% in LPJ-GUESS), temperature (from 21% in LPJ-GUESS to 46% in UVic), and precipitation (from 25% in JULES to 46% in UVic) changes. There were large spikes in CO_2 effects in 2000 (Figures 7b, 7e, and 7h), which were caused by the extremely low GPP in the R01 simulation from the ORCHIDEE model.

4. Discussion

4.1. Disagreement on Carbon Use Efficiency Among Models

Although many previous model intercomparison projects and benchmarking studies have attempted to quantify the importance of model uncertainty for GPP in estimating global carbon budget [*Anav et al.*, 2013; *Piao et al.*, 2013; *Peng et al.*, 2015; *Rawlins et al.*, 2015], our analyses indicate that CUE varied among models in permafrost regions. The higher CUE in the models (54 ± 9%; ±SD among models) than calculated from the gridded database (Figure 3a) and forest sites (Figure 3b) suggest an overestimation of CUE by the models in permafrost regions. More information on CUE of different vegetation or biome types is needed, and the development of a global database of CUE would be helpful for more completely evaluating the accuracy of CUE simulated by models. It should be noted that the regional CUE is calculated from two independent data products, which may generate uncertainty for estimating the CUE. However, a recent global analysis [*Campioli et al.*, 2015] showed that CUE in natural ecosystems globally converges on 46 ± 1%, which is close to the estimates from MODIS/JU11 (47 ± 0%) and site level observations (45 ± 4%) reported in this study.

This study found a very low interannual variability of CUE in most models (Figure 3), but some observational studies have reported substantial interannual variability in CUE [*Campioli et al.*, 2011; *Zhang et al.*, 2014]. In fact, there is evidence showing that the temporal decreasing trend in global CUE is associated with increasing temperature [*Zhang et al.*, 2014] and that CUE increases with higher nitrogen availability [*Chen et al.*, 2013; *Vicca et al.*, 2012] and human management [*Campioli et al.*, 2015]. None of the models in this study use fixed CUE, and the CUE from each model is collectively determined by GPP and autotrophic respiration, including maintenance and growth respiration (Table S1). As shown by Table S1, the simulations of maintenance and growth respiration vary greatly among models. In general, because simulated maintenance and growth respiration are strongly determined by plant biomass, they could be affected by the parameterization of the V_{cmax} indirectly. This study found a positive correlation between CUE and V_{cmax_25} among most models (Figure 4). This could

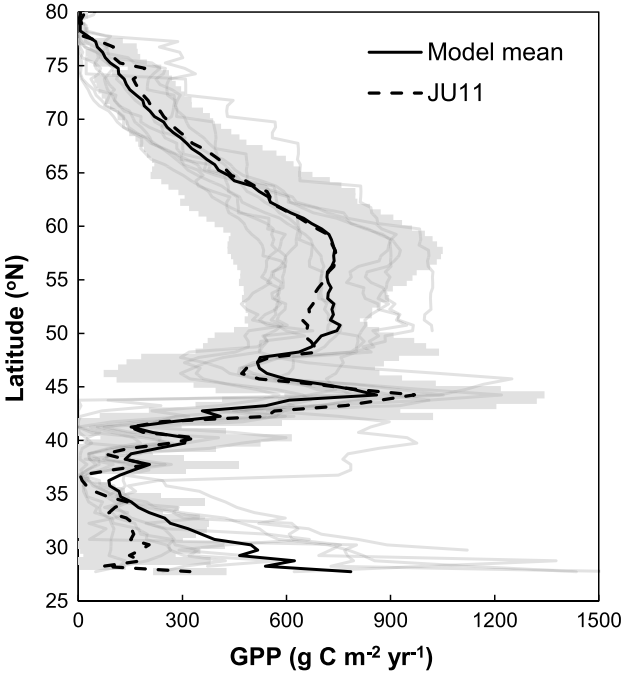


Figure 6. Latitudinal gradients of GPP estimates from the models in this study and the JU11 data product. The bold line shows the multimodel mean, while the grey lines show results from individual models. The shaded gray area is the calculated standard deviation of GPP from JU11 data.

due to an increasing V_{cmax_25} directly enhancing leaf level photosynthesis but only indirectly affecting respiration via vegetation growth in most models (Table S1). Although our understanding of the intermodel differences in CUE is limited by the lack of detailed outputs for all elements in the equations in Table S1, those equations provide useful information for the potential causes. For example, although models (i.e., JULES, CoLM, TEM6, and UVic) simulated the growth respiration based on the scheme of "TRIFFID" global dynamic vegetation model [*Cox*, 2001], they still use different coefficients (e.g., 25% for JULES, CoLM, and UVic but 20% for TEM6). The ORCHIDEE model calculates growth respiration as a fraction (28%) of the remaining allocatable biomass, whereas CLM4.5 calculates growth respiration as 30% of the total carbon in new growth (Table S1). The lowest CUE in TEM6 could result from

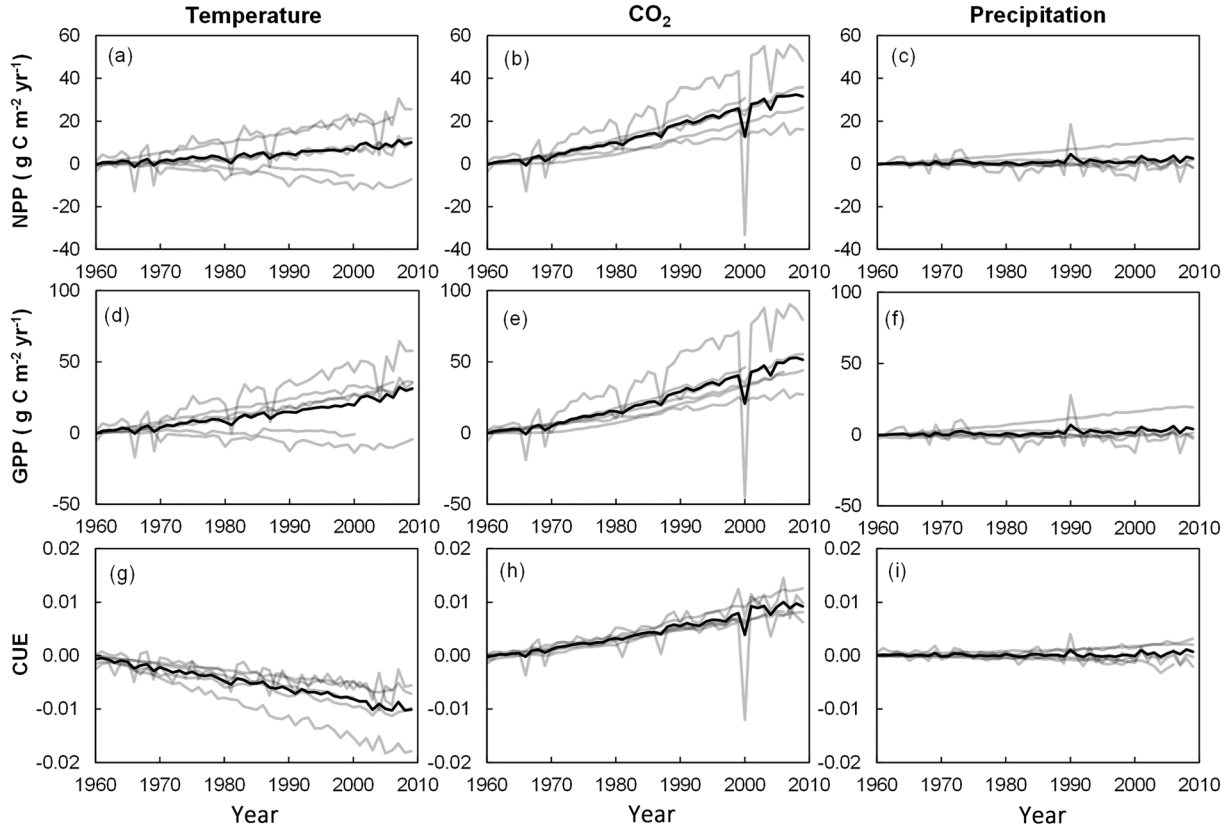


Figure 7. The impacts of air temperature, atmospheric CO_2, and precipitation on (a–c) NPP, (d–f) GPP, and (g–i) CUE over 1960–2009. The gray lines are individual model results (note that only 6 out of the 10 models have done the R02–R04 simulations; Table 1) and the bold black line is the ensemble model mean.

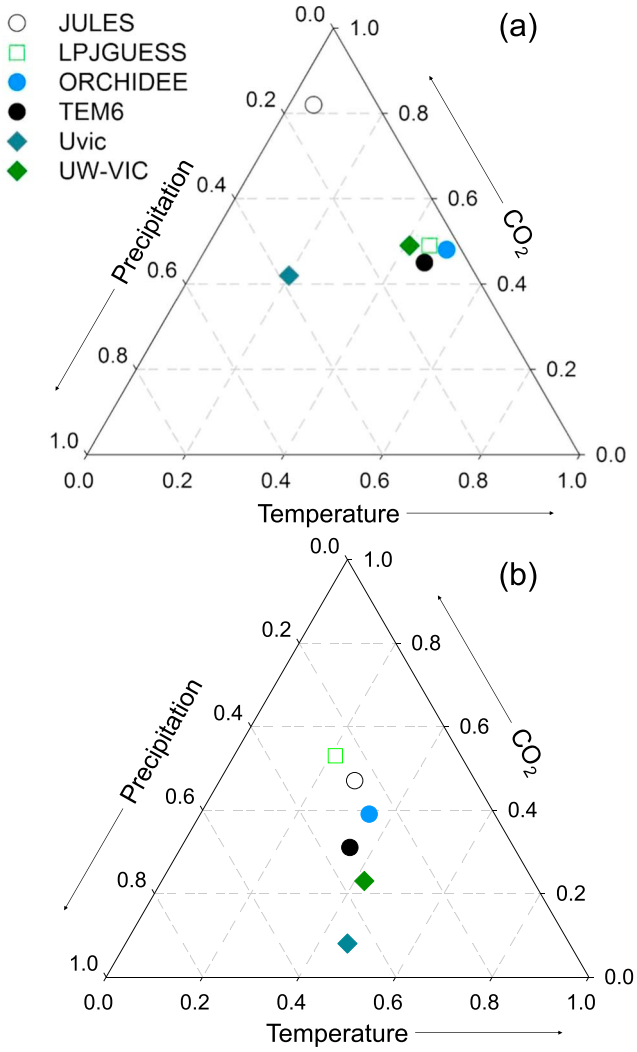


Figure 8. The relative contributions of air temperature, atmospheric CO_2, and precipitation change to dynamics of (a) GPP and (b) CUE from 1960 to 2009.

the large impact of temperature on maintenance respiration (Figure S4), and the relatively low CUE in CLM4.5 could be partially caused by the large fraction of assimilated carbon allocated to growth respiration (Table S1).

The coefficients in the equations for maintenance and growth respiration as well as V_{cmax} (Table S1) have been elucidated in a number of previous ecological studies, but they still act as a large source of uncertainty in most model intercomparison analyses, including the current study. As summarized by *Atkin et al*. [2014], several causes are responsible for the simplistic representation of plant respiration in terrestrial ecosystem models, including the limited data availability describing the regulating mechanisms of plant respiration [*Wright et al*., 2006] and the unclear responses of plant respiration to climate changes [*Huntingford et al*., 2013; *Kornfeld et al*., 2013; *Liang et al*., 2013]. Thus, more research is still needed on how to incorporate into models the underlying mechanisms regulating variability of plant respiration and therefore CUE. For example, the temperature impact on the sink-limited plant growth [*Korner*, 2003; *Wan et al*., 2009; *Fatichi et al*., 2014] is probably an important process missing in models, and it should lower CUE compared to source-based allocation of GPP to growth. Another example is the exploration of the variable relationships among plant traits, e.g., leaf nitrogen concentration, V_{cmax}, and plant respiration [*Kattge et al*., 2009; *Reich et al*., 2009; *Atkin et al*., 2015], which could be helpful to constrain the key parameters of canopy carbon dynamics in the models [*Wang et al*., 2011].

4.2. High Uncertainty in Simulated GPP During Summer and at Lower Latitudes

The highly variable summer GPP_{max} among models could be collectively determined by the uncertain parameterizations of leaf area dynamics and the maximum rate of carboxylation (i.e., V_{cmax}) (Table S1). In this study, the large variation in GPP_{max} among models mainly results from that in SLA but not V_{cmax_25} (Figure 4), but it does not mean that GPP simply varies with SLA. For example, the CoLM has large SLA but relatively low GPP because of its strong temperature limitation (Figure S5) and the additional water constraint in the estimate of V_{cmax} (Table S1). The CLM4.5 model has high V_{cmax_25} but low SLA, leading to its intermediate GPP_{max} among the models. The high GPP_{max} with intermediate V_{cmax_25} in the ORCHIDEE model could result from the limitation of V_{cmax} by age but not by other environmental factors (Table S1) [*Krinner et al*., 2005].

The models have a comparable ensemble mean GPP to the flux tower-based data across the permafrost region (Figure S6), but there is a fourfold difference among models at lower latitude areas, and in particular for the Tibetan Plateau (ranges from about 29°N to 40°N; Figure 6). Although the "Other" permafrost region,

Table 2. A Brief Description of Driving Variables for the 10 Models

Model Name	Climate Data	Disturbance	Land Use	Time Step
CLM45	CRUNCEP4[a]	Fire	Yes	30 min
CoLM	Princeton[b]	Fire	No	30 min
ISBA	WATCH (1901–1978)[c] and WFDEI (1978–2009)[d]	No	No	1 h
JULES	WATCH (1901–2001)[c]	No	No	30 min
LPJ-GUESS	CRU TS3.1[e]	Fire	No	1 day
MIROC-ESM	CMIP5 Drivers[f]	No	No	30 min
ORCHIDEE	WATCH (1901–1978)[c] and WFDEI (1978–2009)[d]	No	Yes	30 min
TEM6	CRUNCEP4[a]	Fire	No	1 month
UVic	CRUNCEP4[a]	No	Yes	1 h
UW-VIC	CRU[g] and UDel[h]	No	No	3 h

[a]Viovy and Ciais (http://dods.extra.cea.fr/).
[b]*Sheffield et al.* [2006] (http://hydrology.princeton.edu/data.pgf.php).
[c]*Weedon et al.* [2011] (http://www.waterandclimatechange.eu/about/watch-forcing-data-20th-century).
[d]http://www.eu-watch.org/gfx_content/documents/README-WFDEI.pdf.
[e]*Harris et al.* [2014], University of East Anglia Climate Research Unit (2013).
[f]*Watanabe et al.* [2011].
[g]Temperature from *Mitchell and Jones* [2005].
[h]*Willmott and Matsuura* [2001] for wind speed and precipitation with corrections [see *Bohn et al.*, 2013a, 2013b].

mostly the Tibetan Plateau, only contributes to about 7% of the area-weighted GPP over permafrost region in the Northern Hemisphere, its contributions to GPP variation (about 21%; Figure S2d) and ensemble model bias (Figure S3d) are both high. It is important to note that no flux site from the Tibetan Plateau was used with the MTE approach in the JU11 GPP database [*Jung et al.*, 2009; *Beer et al.*, 2010]. Given that the environmental dependence of plant photosynthesis is strongly regulated by vegetation type and local climate [*Piao et al.*, 2013; *Liang et al.*, 2013], the JU11 data itself may have large uncertainty in the Tibetan Plateau. Thus, our confidence in the global GPP data products will be enhanced if they can incorporate more flux sites from areas that represent data gaps, e.g., the Tibetan Plateau [*Yu et al.*, 2006; *Zhu et al.*, 2014]. The higher GPP in models than JU11 data at areas around 35°N has also been revealed in the CMIP5 models [*Shao et al.*, 2013], suggesting that more research efforts are still needed in this region. A higher modeled GPP than the JU11 data has been widely reported by various model intercomparison projects in the tropics [*Anav et al.*, 2013] and at the global scale [*Anav et al.*, 2013; *Piao et al.*, 2013; *Shao et al.*, 2013], but this pattern was not found in the northern permafrost regions by this study nor for the CMIP5 models [*Shao et al.*, 2013]. However, we recommend more observations at high latitudes since flux sites are unevenly distributed over the globe and very few sites are located within the northern permafrost domain [*Schimel et al.*, 2015].

Since the climate forcings between models (Table 2) and JU11 data product [*Jung et al.*, 2009, 2011] are similar, the spatial difference in GPP among models and JU11 data could not result from differences in the climate forcings. However, the variation in productivity among models could be largely attributed to their different representations of plant functional types (PFT) across the permafrost region (Figure S1). Since key parameters in photosynthesis algorithms used by most models in this study, e.g., SLA and V_{cmax_25}, are usually fixed based on PFT (Table S1), the different distributions of PFTs generate diverse spatial patterns of SLA and V_{cmax_25} (Figure S7). For example, the greatest GPP from ORCHIDEE among the 10 models largely results from its high SLA (0.026; Table S2 and Figure S7d) and large distribution of boreal deciduous broadleaf forest at high latitudes (Figure S1). In contrast, the low GPP in LPJ-GUESS is strongly determined by its small SLA (0.0093; Table S1 and Figure S7c) and the large area of needleleaf evergreen forest. Thus, a standard vegetation or land cover map with accurate photosynthetic parameters would be valuable for reducing uncertainty in modeled productivity in the permafrost region.

4.3. Vulnerability of NPP to Temperature, CO_2, and Precipitation Changes

There are large differences in the sensitivities of GPP and CUE to changes in air temperature, atmospheric CO_2, and precipitation among models (Figures 7 and 8). The trends in GPP of LPJ-GUESS, ORCHIDEE, TEM6, and UW-Vic are collectively driven by changes in atmospheric CO_2 and air temperature, while the increase in GPP by JULES is mainly driven by the enrichment of atmospheric CO_2. The sensitivity of GPP to precipitation change is more sensitive in UVic than in other models (Figure 8). The high GPP sensitivities to the CO_2

change by LPJ-GUESS, ORCHIDEE, and JULES have been reported in other model intercomparison projects [*Piao et al*., 2013; *Mystakidis et al*., 2017]. Although the results of sensitivity analyses are not available for some models (CLM4.5, CoLM, ISBA, and MIROESM) in this study, their sensitivities have been evaluated by previous studies. For example, MIROESM has similar strength of climate-carbon feedback as ORCHIDEE and JULES, but its sensitivity of land C storage to atmospheric CO_2 change is much smaller [*Mystakidis et al*., 2017]. The sensitivity of land C storage to changes in climate and atmospheric CO_2 changes by CLM4.5 is relatively weak among the CMIP5 models [*Arora et al*., 2013; *Mystakidis et al*., 2017]. For the four models (LPJ-GUESS, ORCHIDEE, TEM6, and UW-Vic) with similar sensitivity to climate and CO_2 changes, they simulate different CUE sensitivities (Figure 8b). This implies that their different sensitivities of NPP trend to climate and CO_2 changes could be largely determined by the differences in their representation of plant respiration.

Evidence for the positive impact of climate warming on vegetation growth and NPP have been widely reported in permafrost regions [*Chapin et al*., 1995; *Hobbie and Chapin*, 1998; *Arft et al*., 1999; *Lin et al*., 2010; *Natali et al*., 2012; *Xia et al*., 2014]. However, the impact of elevated CO_2 on NPP is found to be positive [*Grulke et al*., 1990] or neutral [*Oberbauer et al*., 1986; *Schappi and Korner*, 1996; *Korner et al*., 1997; *Inauen et al*., 2012] in northern permafrost regions. This neutral response could largely be due to nitrogen limitation on the CO_2 effect on NPP, which was widely reported in many temperate ecosystems [*Luo et al*., 2004; *Finzi et al*., 2006; *Reich et al*., 2006; *Norby et al*., 2010] and is more generally observed across a broad array of ecosystems [*McGuire et al*., 1995]. Globally, it is clear that plant production is more limited by nitrogen availability in tundra and boreal ecosystems than in temperate and tropical ecosystems [*Chapin et al*., 1986; *Vitousek and Howarth*, 1991], and it has been inferred that the response of NPP to elevated CO_2 should be more constrained in boreal and tundra ecosystems than in temperate and tropical ecosystems [*McGuire et al*., 1997].

Indeed, modeling studies that have analyzed local and regional responses of models in which GPP is constrained by nitrogen availability indicate that the CO_2 response of GPP in tundra and boreal ecosystems is substantially constrained by nitrogen availability [*McGuire et al*., 1997; *Clein et al*., 2000; *Koven et al*., 2015]. In this study, only two models (CLM4.5 and TEM6) incorporated coupled carbon-nitrogen cycles and another two models (LPJ-GUESS and UW-VIC) have nitrogen limitation on photosynthesis (Table 1). However, among the models that represent nitrogen limitation of productivity, the productivity response to elevated CO_2 for 1960–2009 is not significantly different from that of the models that do not represent nitrogen limitation. Clearly, the influence of nitrogen availability on production in general and on the response of production to changes in atmospheric CO_2 concentration in particular is not adequately constrained by observations. Part of the reason for this is that the role of nitrogen availability on the response of high-latitude plant growth and NPP to increases in atmospheric CO_2 has received very little experimental attention in tundra and boreal forest compared to temperate ecosystems [*Norby et al*., 2015]. Because model responses of biogeochemistry in the northern permafrost region depend substantially on the response of NPP to increases in CO_2, more experimental data are needed to adequately constrain model responses.

Experimental studies or data-based analyses about CO_2 impacts on CUE do not exist for ecosystems in the northern permafrost region. However, a recent modeling study has shown that elevated CO_2 increases C allocation to woody biomass, which has lower respiratory demand than leaves and roots [*De Kauwe et al*., 2014]. The CO_2-induced change in C allocation could increase CUE in the model, though experimental evidence from a desert ecosystem [*Cheng et al*., 2000] showed that CUE might be invariant under elevated CO_2. The unclear trend of either GPP or CUE in response to regional change in annual precipitation (Figures 7f and 7i) contrasts with some recent findings of increasing drought stress and associated vegetation browning or productivity declines with climate warming at high latitudes [*Zhang et al*., 2008; *Beck and Goetz*, 2011; *Bhatt et al*., 2013; *Jeong et al*., 2013]. One potential reason could be the poor representation of vegetation phenology in the models. It has been reported that spring phenology is critical in controlling the annual productivity at temperate and high latitudes [*Richardson et al*., 2010; *Piao et al*., 2011; *Xia et al*., 2014, 2015], and increasing drought stress in spring could negatively affect annual GPP via affecting spring phenology [*Yi et al*., 2014; *Xia et al*., 2014]. However, most models in this study simulate vegetation phenology with thermal conditions [*Richardson et al*., 2012] but neglect the role of water availability. Also, either increasing [e.g., *Niu et al*., 2012] or declining [e.g., *Ciais et al*., 2005] GPP_{max} with rising temperature has been reported by analyses with eddy flux data, suggesting that more knowledge about the PFT-specific optimal temperatures for plant photosynthesis and their covariations with temperature change is needed in the permafrost region.

4.4. Limitations of Current Model Intercomparison Analyses

Although multiple processes that determine NPP uncertainty have been discussed in this study, the experimental design of this model intercomparison project did not allow us to do comprehensive evaluations. Thus, this study has some limitations that should be addressed by future observational and modeling efforts.

First, CUE is highly variable among models but nearly invariant within models, suggesting that more measurements and analyses are needed to quantify the ranges of CUE and its dynamics in the permafrost region. It should be noted that CUE is not only directly affected by GPP and respiration but also directly influenced by the allocation of NPP (e.g., more NPP allocation to leaf tends to increase CUE via more photosynthetic than respiratory tissues). Given the poor representation of allocation in current models [*De Kauwe et al*., 2014], variation in allocation could be an important contribution to the variation in CUE among models.

Second, large differences in the distributions of PFTs and their associated photosynthetic parameters exist among the models. The contribution of the different PFT maps to the uncertainty of modeled C cycle needs to be better quantified.

Third, the models in this study simulate very high production in permafrost regions, which could partly be the result of the lack of nutrient limitation on productivity in most models.

Fourth, the global data sets used in this study have large uncertainty. For example, both data products of MODIS and JU11 rely heavily on the fractional photosynthetically active radiation (FPAR) absorbed by the canopy, while environmental changes such as the CO_2 elevation affect NPP via increasing light-use efficiency [*De Kauwe et al*., 2016]. How the impact of FPAR on NPP differs between data products and model outputs has not been comprehensively evaluated in this study.

Lastly, long-term CO_2 flux measurements by eddy flux towers have been widely used for benchmarking models. Interannual variability [*Keenan et al*., 2012] and seasonality [*Peng et al*., 2015] of measured GPP by flux towers are useful ecosystem properties for diagnosing simulated environmental impacts on GPP by models. For example, the ORCHIDEE model has larger interannual variability of NPP (Figure 2) and a larger response to climate change than other models in this study, which could be further evaluated at the site level if there are more long-term observations. However, as shown by the recent release of FLUXNET2015 data set (http://fluxnet.fluxdata.org/data/fluxnet2015-dataset/), there are only a few eddy flux towers providing >10 years measurements in the permafrost region. Thus, when the flux measurements become richer in the permafrost region, a comparison of model performance against flux data between extremely warm and cool years would be insightful for improving the simulation of NPP in the permafrost region.

5. Conclusion

It is critical to reduce the uncertainty of NPP estimates in the northern permafrost region for making better projections of the permafrost carbon feedback to climate change. This study found that the large NPP uncertainty in current models stems from not only GPP but also CUE. The ensemble mean GPP among models is slightly higher than the flux-based estimate, which is largely associated with the higher simulated GPP that was simulated by ORCHIDEE in comparison to other models. The large intermodel variation in CUE has not been sufficiently studied in previous model evaluations. Reducing such uncertainty is challenging because the models have different structures (Table S1), parameters (Table S2), and representations of PFTs (Figure S1) for simulating key processes of NPP in the permafrost regions. Models also disagree with each other on the contributions of environmental factors toward increasing NPP during between 1960 and 2009. Thus, systematic approaches that link C processes and environmental factors should be used for diagnosing terrestrial C cycle issues in models. Overall, the modeling of the global C cycle will be greatly improved with databases of estimated productivity and better understanding of the environmental regulation of both GPP and CUE dynamics in the northern permafrost region.

Acknowledgments
The authors thank John Kimball for his constructive suggestions on the earlier version of this manuscript. This study was developed as part of the modeling integration team of the Permafrost Carbon Network (PCN, www.permafrostcarbon.org) funded by the National Science Foundation and the U.S. Geological Survey. Research in Y. L. Ecolab was financially supported by the U.S. Department of Energy (DE SC0008270 and DE-SC00114085) and the U.S. National Science Foundation (NSF) grants EF 1137293 and OIA-1301789. J.X. was also supported by the National 1000 Young Talents Program of China. E.B., S.P., P.C., I.G., and G.K. acknowledge financial support by the European Union Seventh Framework Programme (FP7/2007-2013) project PAGE21, under GA282700. Any use of trade, firm, or product names is for descriptive purposes only and does not imply endorsement by the U.S. Government. The simulation data analyzed in this manuscript are available through the National Snow and Ice Data Center through e-mail request to Kevin Schaefer (kevin.schaefer@nsidc.org).

References

Anav, A., P. Friedlingstein, M. Kidston, L. Bopp, P. Ciais, P. Cox, C. Jones, M. Jung, R. Myneni, and Z. Zhu (2013), Evaluating the land and ocean components of the global carbon cycle in the CMIP5 Earth System Models, *J. Clim.*, *26*, 6801–6843.

Arft, A., et al. (1999), Responses of tundra plants to experimental warming: Meta-analysis of the international tundra experiment, *Ecol. Monogr.*, *69*, 491–511.

Arora, V. K., et al. (2013), Carbon-concentration and carbon-climate feedbacks in CMIP5 Earth system models, *J. Clim.*, *26*, 5289–5314.

Atkin, O. K., P. Meir, and M. H. Turnbull (2014), Improving representation of leaf respiration in large-scale predictive climate–vegetation models, *New Phytol.*, *202*, 743–748.
Atkin, O. K., et al. (2015), Global variability in leaf respiration in relation to climate, plant functional types and leaf traits, *New Phytol.*, *206*, 614–636.
Baldocchi, D., et al. (2001), FLUXNET: A new tool to study the temporal and spatial variability of ecosystem-scale carbon dioxide, water vapor, and energy flux densities, *Bull. Am. Meteorol. Soc.*, *82*, 2415–2434.
Beck, P. S. A., and S. J. Goetz (2011), Satellite observations of high northern latitude vegetation productivity changes between 1982 and 2008: Ecological variability and regional differences, *Environ. Res. Lett.*, *14*(4), 373–379.
Beer, C., et al. (2010), Terrestrial gross carbon dioxide uptake: Global distribution and covariation with climate, *Science*, *329*, 834–838.
Belmaker, J., and W. Jetz (2015), Relative roles of ecological and energetic constraints, diversification rates and region history on global species richness gradients, *Ecol. Lett.*, *18*, 563–571.
Bhatt, U. S., D. A. Walker, M. K. Raynolds, P. A. Bieniek, H. E. Epstein, J. C. Comiso, J. E. Pinzon, C. J. Tucker, and I. V. Polyakov (2013), Recent declines in warming and vegetation greening trends over Pan-Arctic Tundra, *Remote Sens.*, *5*(9), 4229–4254.
Bohn, T., D. Lettenmaier, K. Sathulur, L. Bowling, E. Podest, K. Mcdonald, and T. Friborg (2007), Methane emissions from western Siberian wetlands: Heterogeneity and sensitivity to climate change, *Environ. Res. Lett.*, *2*, 045,015.
Bradford, M. A., and T. W. Crowther (2013), Carbon use efficiency and storage in terrestrial ecosystems, *New Phytol.*, *199*, 7–9.
Bohn, T. J., B. Livneh, J. W. Oyler, S. W. Running, B. Nijssen, and D. P. Lettenmaier (2013a), Global evaluation of MTCLIM and related algorithms for forcing of ecological and hydrological models, *Agric. For. Meteorol.*, *176*, 38–49.
Bohn, T. J., et al. (2013b), Modeling the large-scale effects of surface moisture heterogeneity on wetland carbon fluxes in the West Siberian Lowland, *Biogeosciences*, *10*, 6559–6576.
Campioli, M., B. Gielen, M. Göckede, D. Papale, O. Bouriaud, and A. Granier (2011), Temporal variability of the NPP-GPP ratio at seasonal and interannual time scales in a temperate beech forest, *Biogeosciences*, *8*, 2481–2492.
Campioli, M., et al. (2015), Biomass production efficiency controlled by management in temperate and boreal ecosystems, *Nat. Geosci.*, *8*, 843–846.
Chapin, F. S., III, P. M. Vitousek, and K. Van Cleve (1986), The nature of nutrient limitation in plant communities, *Am. Nat.*, *127*(48–58), 1986.
Chapin, F. S., III, G. R. Shaver, A. E. Giblin, K. J. Nadelhoffer, and J. A. Laundre (1995), Responses of arctic tundra to experimental and observed changes in climate, *Ecology*, *76*, 694–711.
Chen, G. S., Y. S. Yang, and D. Robinson (2013), Allocation of gross primary production in forest ecosystems: Allometric constraints and environmental responses, *New Phytol.*, *200*, 1176–1186.
Cheng, W. X., D. A. Sims, Y. Q. Luo, J. S. Coleman, and D. W. Johnson (2000), Photosynthesis, respiration, and net primary production of sunflower stands in ambient and elevated atmospheric CO_2 concentrations: An invariant NPP: GPP ratio?, *Global Change Biol.*, *6*, 931–941.
Ciais, P., et al. (2005), Europe-wide reduction in primary productivity caused by the heat and drought in 2003, *Nature*, *437*, 529–533.
Clark, D., et al. (2011), The Joint UK Land Environment Simulator (JULES), model description–Part 2: Carbon fluxes and vegetation dynamics, *Geosci. Model Dev.*, *4*, 701–722.
Clein, J., B. Kwiatkowski, A. D. McGuire, J. E. Hobbie, E. B. Rastetter, J. M. Melillo, and D. W. Kicklighter (2000), Modeling carbon responses of tundra ecosystems to historical and projected climate: A comparison of a plot- and a global-scale ecosystem model to identify process-based uncertainties, *Global Change Biol.*, *6*, S127–S140.
Cox, P. M. (2001), Description of the TRIFFID dynamic global vegetation model, Technical Note 24, Hadley Centre, United Kingdom Meteorol. Office, Bracknell, U. K.
Cramer, W., D. W. Kicklighter, A. Bondeau, B. M. Iii, G. Churkina, B. Nemry, A. Ruimy, and A. L. Schloss (1999), Comparing global models of terrestrial net primary productivity (NPP): Overview and key results, *Global Change Biol.*, *5*, 1–15.
Dai, Y. J., et al. (2003), The Common Land Model, *Bull. Am. Meteorol. Soc.*, *84*, 1013–1023.
De Kauwe, M. G., et al. (2014), Where does the carbon go? A model-data intercomparison of vegetation carbon allocation and turnover processes at two temperate forest free-air CO_2 enrichment sites, *New Phytol.*, *203*, 883–899.
De Kauwe, M. G., T. F. Keenan, B. E. Medlyn, I. C. Prentice, and C. Terrer (2016), Satellite based estimates underestimate the effect of CO_2 fertilization on net primary productivity, *Nat. Clim. Change*, *6*, 892–893.
Delucia, E. H., J. E. Drake, R. B. Thomas, and M. Gonzalez-Meler (2007), Forest carbon use efficiency: Is respiration a constant fraction of gross primary production?, *Global Change Biol.*, *13*, 1157–1167.
Dillaway, D. N., and E. L. Kruger (2014), Trends in seedling growth and carbon-use efficiency vary among broadleaf tree species along a latitudinal transect in eastern North America, *Global Change Biol.*, *20*, 908–922.
Fatichi, S., S. Leuzinger, and C. Körner (2014), Moving beyond photosynthesis: From carbon source to sink-driven vegetation modeling, *New Phytol.*, *201*, 1086–1095.
Fernandez-Martinez, M., et al. (2015), Nutrient availability as the key regulator of global forest carbon balance, *Nat. Clim. Change*, *4*, 471–476.
Finzi, A. C., et al. (2006), Progressive nitrogen limitation of ecosystem processes under elevated CO_2 in a warm-temperate forest, *Ecology*, *87*, 15–25.
Friedlingstein, P., M. Meinshausen, V. K. Arora, C. D. Jones, A. Anav, S. K. Liddicoat, and R. Knutti (2013), Uncertainties in CMIP5 climate projections due to carbon cycle feedbacks, *J. Clim.*, *27*, 511–526.
Gibelin, A. L., J. C. Calvet, J. L. Roujean, L. Jarlan, and S. O. Los (2006), Ability of the land surface model ISBA-A-gs to simulate leaf area index at the global scale: Comparison with satellites products, *J. Geophys. Res.*, *111*, D18102, doi:10.1029/2005JD006691.
Gromping, U. (2006), Relative importance for linear regression in R: The package relaimpo, *J. Stat. Soft.*, *17*. [Available at http://www.jstatsoft.org/v17/i01.]
Grulke, N., G. Riechers, W. Oechel, U. T. Hjelm, and C. Jaeger (1990), Carbon balance in tussock tundra under ambient and elevated atmospheric CO_2, *Oecologia*, *83*, 485–494.
Hajima, T., K. Tachiiri, A. Ito, and M. Kawamiya (2014), Uncertainty of concentration–terrestrial carbon feedback in Earth system models, *J. Clim.*, *27*, 3425–3445.
Harris, I., P. D. Jones, T. J. Osborn, and D. H. Lister (2014), Updated high-resolution grids of monthly climatic observations, *Int. J. Climatol.*, *34*, 623–642.
Hayes, D. J., A. D. McGuire, D. W. Kicklighter, K. R. Gurney, T. J. Burnside, and J. M. Melillo (2011), Is the northern high latitude land-based CO_2 sink weakening?, *Global Biogeochem. Cycles*, *25*, GB3018, doi:10.1029/2010GB003813.
Heinsch, F. A., et al. (2003), GPP and NPP (MOD17A2/A3) Products NASA MODIS Land Algorithm, MOD17 User's Guide, 1-57.
Hobbie, S. E., and F. S. Chapin III (1998), The response of tundra plant biomass, aboveground production, nitrogen, and CO_2 flux to experimental warming, *Ecology*, *79*, 1526–1544.

Huntingford, C., et al. (2013), Simulated resilience of tropical rainforests to CO_2-induced climate change, *Nat. Geosci.*, *6*, 268–273.
Inauen, N., C. Korner, and E. Hiltbrunner (2012), No growth stimulation by CO_2 enrichment in alpine glacier forefield plants, *Global Change Biol.*, *18*, 985–999.
Jeong, S. J., C. H. Ho, B. M. Kim, S. Feng, and D. Medvigy (2013), Non-linear response of vegetation to coherent warming over northern high latitudes, *Remote Sens. Lett.*, *4*(2), 123–130.
Ji, D., et al. (2014), Description and basic evaluation of Beijing Normal University Earth System Model (BNU-ESM) version 1, *Geosci. Model Dev.*, *7*, 2039–2064.
Jung, M., M. Reichstein, and A. Bondeau (2009), Towards global empirical upscaling of FLUXNET eddy covariance observations: Validation of a model tree ensemble approach using a biosphere model, *Biogeosciences*, *6*, 2001–2013.
Jung, M., et al. (2011), Global patterns of land-atmosphere fluxes of carbon dioxide, latent heat, and sensible heat derived from eddy covariance, satellite, and meteorological observations, *J. Geophys. Res.*, *117*, G00J07, doi:10.1029/2010JG001566.
Kattge, J., W. Knorr, T. Raddatz, and C. Wirth (2009), Quantifying photosynthetic capacity and its relationship to leaf nitrogen content for global-scale terrestrial biosphere models, *Global Change Biol.*, *15*, 976–991.
Keenan, T. F., et al. (2012), Terrestrial biosphere model performance for inter-annual variability of land-atmosphere CO_2 exchange, *Global Change Biol.*, *18*, 1971–1987.
Knorr, W. (2000), Annual and interannual CO_2 exchanges of the terrestrial biosphere: Process-based simulations and uncertainties, *Global Ecol. Biogeogr.*, *9*, 225–252.
Korner, C. (2003), Carbon limitation in trees, *J. Ecol.*, *91*, 4–17.
Korner, C., M. Diemer, B. Schappi, P. Niklaus, and J. Arnone (1997), The responses of alpine grassland to four seasons of CO_2 enrichment: A synthesis, *Acta Oecologica*, *18*, 165–175.
Kornfeld, A., M. Heskel, O. K. Atkin, L. Gough, K. L. Griffin, T. W. Horton, and M. H. Turnbull (2013), Respiratory flexibility and efficiency are affected by simulated global change in Arctic plants, *New Phytol.*, *197*, 1161–1172.
Koven, C. D., B. Ringeval, P. Friedlingstein, P. Ciais, P. Cadule, D. Khvorostyanov, G. Krinner, and C. Tarnocai (2011), Permafrost carbon-climate feedbacks accelerate global warming, *Proc. Natl. Acad. Sci. U.S.A.*, *108*, 14,769–14,774.
Koven, C. D., W. J. Riley, and A. Stern (2013), Analysis of permafrost thermal dynamics and response to climate change in the CMIP5 earth system models, *J. Clim.*, *26*, 1877–1900.
Koven, C. D., D. M. Lawrence, and W. J. Riley (2015), Permafrost carbon-climate feedback is sensitive to deep soil carbon decomposability but not deep soil nitrogen dynamics, *Proc. Natl. Acad. Sci. U.S.A.*, *112*, 3752–3757.
Krinner, G., N. Viovy, N. De Noblet-Ducoudre, J. Ogée, J. Polcher, P. Friedlingstein, P. Ciais, S. Sitch, and I. C. Prentice (2005), A dynamic global vegetation model for studies of the coupled atmosphere-biosphere system, *Global Biogeochem. Cycles*, *19*, GB1015, doi:10.1029/2003GB002199.
Liang, J. Y., J. Y. Xia, L. L. Liu, and S. Q. Wan (2013), Global patterns of the responses of leaf-level photosynthesis and respiration in terrestrial plants to experimental warming, *J. Plant Ecol.*, *6*, 437–447.
Lin, D. L., J. Y. Xia, and S. Q. Wan (2010), Climate warming and biomass accumulation of terrestrial plants: A meta-analysis, *New Phytol.*, *188*, 187–198.
Lindeman, R. H., P. F. Merenda, and R. Z. Gold (1980), *Introduction to Bivariate and Multivariate Analysis*, Scott, Foresman Glenview, Ill.
Litton, C. M., J. W. Raich, and M. G. Ryan (2007), Carbon allocation in forest ecosystems, *Global Change Biol.*, *13*, 2089–2109.
Luo, Y., et al. (2004), Progressive nitrogen limitation of ecosystem responses to rising atmospheric carbon dioxide, *BioScience*, *54*, 731–739.
Luyssaert, S., et al. (2007), CO_2 balance of boreal, temperate, and tropical forests derived from a global database, *Global Change Biol.*, *13*, 2509–2537.
Mao, D., L. Luo, Z. Wang, C. Zhang, and C. Ren (2015), Variations in net primary productivity and its relationships with warming climate in the permafrost zone of the Tibetan Plateau, *J. Geogr. Sci.*, *25*, 967–977.
Matthews, H. D., A. J. Weaver, K. J. Meissner, N. P. Gillett, and M. Eby (2004), Natural and anthropogenic climate change: Incorporating historical land cover change, vegetation dynamics and the global carbon cycle, *Clim. Dyn.*, *22*, 461–479.
McGuire, A. D., J. M. Melillo, and L. A. Joyce (1995), The role of nitrogen in the response of forest net primary production to elevated atmospheric carbon dioxide, *Ann. Rev. Ecol. Syst.*, *26*, 473–503.
McGuire, A. D., J. M. Melillo, D. W. Kicklighter, Y. Pan, X. Xiao, J. Helfrich, B. Moore III, C. J. Vorosmarty, and A. L. Schloss (1997), Equilibrium responses of global net primary production and carbon storage to doubled atmospheric carbon dioxide: Sensitivity to changes in vegetation nitrogen concentration, *Global Biogeochem. Cycles*, *11*, 173–189, doi:10.1029/97GB00059.
McGuire, A. D., L. G. Anderson, T. R. Christensen, S. Dallimore, L. Guo, D. J. Hayes, M. Heimann, T. D. Lorenson, R. W. Macdonald, and N. Roulet (2009), Sensitivity of the carbon cycle in the Arctic to climate change, *Ecol. Monogr.*, *79*, 523–555.
McGuire, A. D., et al. (2010), An analysis of the carbon balance of the Arctic Basin from 1997 to 2006, *Tellus B*, *62*, 455–474.
McGuire, A. D., et al. (2016), A model-based analysis of the vulnerability of carbon in the permafrost region between 1960 and 2009, *Global Biogeochem. Cycles*, *30*, 1015–1037, doi:10.1002/2016GB005405.
McGuire, A. D., et al. (2017), Variability in the sensitivity among model simulations of permafrost and carbon dynamics in the permafrost region between 1960 and 2009, *Global Biogeochem. Cycles.*, *30*, 1015–1037.
Metcalfe, D. B., et al. (2010), Shifts in plant respiration and carbon use efficiency at a large-scale drought experiment in the eastern Amazon, *New Phytol.*, *187*, 608–621.
Mitchell, T. D., and P. D. Jones (2005), An improved method of constructing a database of monthly climate observations and associated high-resolution grids, *Int. J. Climatol.*, *25*(6), 693–712.
Mystakidis, S., S. I. Seneviratne, N. Gruber, and E. L. Davin (2017), Hydrological and biogeochemical constraints on terrestrial carbon cycle feedbacks, *Environ. Res. Lett.*, *12*, 014009.
Natali, S. M., E. G. Schuur, and R. L. Rubin (2012), Increased plant productivity in Alaskan tundra as a result of experimental warming of soil and permafrost, *J. Ecol.*, *100*, 488–498.
Niu, S., et al. (2012), Thermal optimality of net ecosystem exchange of carbon dioxide and underlying mechanisms, *New Phytol.*, *194*, 775–783.
Norby, R. J., J. M. Warren, C. M. Iversen, B. E. Medlyn, and R. E. Mcmurtrie (2010), CO_2 enhancement of forest productivity constrained by limited nitrogen availability, *Proc. Natl. Acad. Sci. U.S.A.*, *107*, 19,368–19,373.
Norby, R. J., et al. (2015), Model-data synthesis for the next generation of forest free-air CO_2 enrichment (FACE) experiments, *New Phytol.*, doi:10.1111/nph.13593.
Oberbauer, S. F., N. Sionit, S. J. Hastings, and W. C. Oechel (1986), Effects of CO_2 enrichment and nutrition on growth, photosynthesis, and nutrient concentration of Alaskan tundra plant species, *Can. J. Bot.*, *64*, 2993–2998.
Oleson, K. W., et al. (2013), Technical description of version 4.5 of the Community Land Model (CLM). NCAR Technical Note.

Olson, R. J., J. M. O. Scurlock, S. D. Prince, D. L. Zheng, K. R. Johnson (2001), *NPP Multi-Biome*, Oak Ridge National Laboratory Distributed Active Archive Center, Oak Ridge, Tenn. [Available at http://www.daac.ornl.gov.]
Papale, D., et al. (2006), Towards a standardized processing of Net Ecosystem Exchange measured with eddy covariance technique: Algorithms and uncertainty estimation, *Biogeosciences*, *3*, 571–583.
Peng, S., et al. (2015), Benchmarking the seasonal cycle of CO_2 fluxes simulated by terrestrial ecosystem models, *Global Biogeochem. Cycles*, *29*, 46–64, doi:10.1002/2014GB004931.
Peng, S., et al. (2016), Simulated high-latitude soil thermal dynamics during the past four decades, *Cryosphere*, *10*, 179–192, doi:10.5194/tcd-9-2301-2015.
Piao, S. L., S. Luyssaert, P. Ciais, I. A. Janssens, A. Chen, C. Cao, J. Fang, P. Friedlingstein, Y. Luo, and S. Wang (2010), Forest annual carbon cost: A global-scale analysis of autotrophic respiration, *Ecology*, *91*, 652–661.
Piao, S. L., M. D. Cui, A. P. Chen, X. H. Wang, P. Ciais, J. Liu, and Y. H. Tang (2011), Altitude and temperature dependence of change in the spring vegetation green-up date from 1982 to 2006 in the Qinghai-Xizang Plateau, *Agric. For. Meteorol.*, *151*(12), 1599–1608.
Piao, S. L., et al. (2013), Evaluation of terrestrial carbon cycle models for their response to climate variability and to CO_2 trends, *Global Change Biol.*, *19*, 2117–2132.
Rawlins, M., et al. (2015), Assessment of model estimates of land-atmosphere CO_2 exchange across northern Eurasia, *Biogeosci. Discuss.*, doi:10.5194/bg-12-1-2015.
Reich, P. B., et al. (2006), Nitrogen limitation constrains sustainability of ecosystem response to CO_2, *Nature*, *440*, 922–925.
Reich, P. B., J. Oleksyn, and I. J. Wright (2009), Leaf phosphorus influences the photosynthesis-nitrogen relation: A cross-biome analysis of 314 species, *Oecologia*, *160*, 207–212.
Richardson, A. D., et al. (2010), Influence of spring and autumn phenological transitions on forest ecosystem productivity, *Philos. Trans. R. Sococ. B*, *365*(1555), 3227–3246.
Richardson, A. D., et al. (2012), Terrestrial biosphere models need better representation of vegetation phenology: Results from the North American Carbon Program Site Synthesis, *Global Change Biol.*, *18*, 566–584.
Running, S. W., and M. Zhao (2015), User's guide: Daily GPP and annual NPP (MOD17A2/A3) products NASA Earth Observing System MODIS land algorithm.
Sato, H., A. Itoh, and T. Kohyama (2007), SEIB-DGVM: A new dynamic global vegetation model using a spatially explicit individual-based approach, *Ecol. Model.*, *200*, 279–307.
Schaefer, K., H. Lantuit, V. E. Romanovsky, E. G. Schuur, and R. Witt (2014), The impact of the permafrost carbon feedback on global climate, *Environ. Res. Lett.*, *9*, 085003.
Schappi, B., and C. Korner (1996), Growth responses of an alpine grassland to elevated CO_2, *Oecologia*, *105*, 43–52.
Schimel, D., et al. (2015), Observing terrestrial ecosystems and the carbon cycle from space, *Global Change Biol.*, *21*, 1762–1776.
Schneider, U., et al. (2008), Global precipitation analysis products of the GPCC, report, Global Precip. Climatol. Cent., Offenbach, Germany.
Schuur, E. G., et al. (2008), Vulnerability of permafrost carbon to climate change: Implications for the global carbon cycle, *Bioscience*, *58*, 701–714.
Schuur, E. G., et al. (2015), Climate change and the permafrost carbon feedback, *Nature*, *520*, 171–179.
Shao, P., X. B. Zeng, K. Sakaguchi, R. K. Monson, and X. D. Zeng (2013), Terrestrial carbon cycle: Climate relations in eight CMIP5 earth system models, *J. Clim.*, *26*, 8744–8764.
Sheffield, J., G. Goteti, and E. F. Wood (2006), Development of a 50-yr high-resolution global dataset of meteorological forcings for land surface modeling, *J. Clim.*, *19*(13), 3088–3111.
Smith, B., I. C. Prentice, and M. T. Sykes (2001), Representation of vegetation dynamics in the modelling of terrestrial ecosystems: Comparing two contrasting approaches within European climate space, *Global Ecol. Biogeogr.*, *10*, 621–637.
Sonnentag, O., G. Van Der Kamp, A. G. Barr, and J. M. Chen (2010), On the relationship between water table depth and water vapor and carbon dioxide fluxes in a minerotrophic fen, *Global Change Biol.*, *16*, 1762–1776.
Tang, J. W., S. Luyssaert, A. D. Richardson, W. Kutsch, and I. A. Janssens (2014), Steeper declines in forest photosynthesis than respiration explain age-driven decreases in forest growth, *Proc. Natl. Acad. Sci. U.S.A.*, *111*, 8856–8860.
Tchebakova, N. M., E. Parfenova, and A. J. Soja (2009), The effects of climate, permafrost and fire on vegetation change in Siberia in a changing climate, *Environ. Res. Lett.*, *4*, 045013.
Tjiputra, J., et al. (2013), Evaluation of the carbon cycle components in the Norwegian Earth System Model (NorESM), *Geosci. Model Dev.*, *6*, 301–325.
Todd-Brown, K., J. Randerson, W. Post, F. Hoffman, C. Tarnocai, E. Schuur, and S. Allison (2013), Causes of variation in soil carbon simulations from CMIP5 Earth system models and comparison with observations, *Biogeosciences*, *10*, 1717–1736.
Tuanmu, M.-N., and W. Jetz (2015), A global, remote sensing-based characterization of terrestrial habitat heterogeneity for biodiversity and ecosystem modelling, *Global Ecol. Biogeogr.*, *24*, 1329–1339.
Turner, D. P., et al. (2006), Evaluation of MODIS NPP and GPP products across multiple biomes, *Remote Sens. Environ.*, *102*, 282–292.
Vicca, S., et al. (2012), Fertile forests produce biomass more efficiently, *Ecol. Lett.*, *15*, 520–526.
Vitousek, P. M., and R. W. Howarth (1991), Nitrogen limitation on land and in the sea: How can it occur?, *Biogeochemistry*, *13*, 87–115.
Wan, S. Q., J. Y. Xia, W. X. Liu, and S. L. Niu (2009), Photosynthetic overcompensation under nocturnal warming enhances grassland carbon sequestration, *Ecology*, *90*, 2700–2710.
Wang, Y. P., X. J. Lu, I. J. Wright, Y. J. Dai, P. J. Rayner, and P. B. Reich (2011), Correlations among leaf traits provide a significant constraint on the estimate of global gross primary production, *Geophys. Res. Lett.*, *39*, L19405, doi:10.1029/2012GL053461.
Watanabe, S., et al. (2011), MIROC-ESM 2010: Model description and basic results of CMIP5-20c3m experiments, *Geosci. Model Dev.*, *4*, 845–872.
Weedon, G. P., S. Gomes, P. Viterbo, W. J. Shuttleworth, E. Blyth, H. Österle, J. C. Adam, N. Bellouin, O. Boucher, and M. Best (2011), Creation of the WATCH Forcing data and its use to assess global and regional reference crop evaporation over land during the twentieth century, *J. Hydrometeorol.*, *12*, 823–848, doi:10.1175/2011JHM1369.1.
Willmott, C. J., and K. Matsuura (2001), Terrestrial air temperature and precipitation: Monthly and annual time series (1950–1999) (version 1.02), Center for Climate Research, Univ. of Delaware, Newark, Del. [Available at http://climate.geog.udel.edu/~climate/html_pages/archive.html.]
Wright, I. J., P. B. Reich, O. K. Atkin, C. H. Lusk, M. G. Tjoelker, and M. Westoby (2006), Irradiance, temperature and rainfall influence leaf dark respiration in woody plants: Evidence from comparisons across 20 sites, *New Phytol.*, *169*, 309–319.
Wu, Z. W., H. S. He, Y. Liang, L. Y. Cai, and B. J. Lewis (2013), Determining relative contributions of vegetation and topography to burn severity from LANDSAT imagery, *Environ. Manage.*, *52*, 821–836.

Xia, J. Y., J. Q. Chen, S. L. Piao, P. Ciais, Y. Q. Luo, and S. Q. Wan (2014), Terrestrial carbon cycle affected by non-uniform climate warming, *Nat. Geosci.*, *7*, 173–180.

Xia, J. Y., et al. (2015), Joint control of terrestrial gross primary productivity by plant phenology and physiology, *Proc. Natl. Acad. Sci. U.S.A.*, *112*, 2788–2793.

Yi, C., J. S. Kimball, and R. H. Reichle (2014), Spring phenology determines summer net carbon uptake in northern ecosystems, *Environ. Res. Lett.*, *9*, 065003.

Yu, G. R., X. F. Wen, X. M. Sun, B. D. Tanner, X. H. Lee, and J. Y. Chen (2006), Overview of ChinaFLUX and evaluation of its eddy covariance measurement, *Agric. For. Meteorol.*, *137*, 125–137.

Zhang, K., J. S. Kimball, E. H. Hogg, M. Zhao, W. C. Oechel, J. J. Cassano, and S. W. Running (2008), Satellite-based model detection of recent climate-driven changes in northern high-latitude vegetation productivity, *J. Geophys. Res.*, *113*, G03033, doi:10.1029/2007JG000621.

Zhang, Y. J., M. Xu, H. Chen, and J. Adams (2009), Global pattern of NPP to GPP ratio derived from MODIS data: Effects of ecosystem type, geographical location and climate, *Global Ecol. Biogeogr.*, *18*, 280–290.

Zhang, Y. J., et al. (2014), Climate-driven global changes in carbon use efficiency, *Global Ecol. Biogeogr.*, *23*, 144–155.

Zhu, X. J., et al. (2014), Geographical statistical assessments of carbon fluxes in terrestrial ecosystems of China: Results from upscaling network observations, *Global Planet. Change*, *118*, 52–61.

Zhuang, Q., et al. (2003), Carbon cycling in extratropical terrestrial ecosystems of the Northern Hemisphere during the 20th Century: A modeling analysis of the influences of soil thermal dynamics, *Tellus*, *55B*, 751–776.